ISSN: 0975-833X

Available online at http://www.journalcra.com

International Journal of Current Research
Vol. 9, Issue, 04, pp.48662-48672, April, 2017

INTERNATIONAL JOURNAL OF CURRENT RESEARCH

RESEARCH ARTICLE

THERMAL ANALYSIS OF BIOMASS/GAS TURBINE AND WIND TURBINE HYBRID SYSTEM FOR ELECTRICITY GENERATION AND DISTRICT HEATING

***Sami, S. and Garzon, J. P.**

Research Center for Renewable Energy, Catholic University of Cuenca, Cuenca, Ecuador

ARTICLE INFO

Article History:
Received 08th January, 2017
Received in revised form
24th February, 2017
Accepted 22nd March, 2017
Published online 20th April, 2017

Key words:

Hybrid System, Wind turbine, Biomass/ gas turbine, district heating, Modeling, Simulation, Validation experimental data.

ABSTRACT

In this paper we present the modeling, simulation and analysis of the energy conversion equations describing the behavior of a hybrid system of wind turbine and biomass/ gas turbine and district heating hybrid system for power generation and district heating. A numerical model based upon the aforementioned equations has been developed, integrated, coded and the results were compared to experimental data. The model fairly predicted with experimental data under various conditions.

Citation: Sami, S. and Garzon, J. P. 2017. "Thermal analysis of biomass/gas turbine and wind turbine hybrid system for electricity generation and district heating", *International Journal of Current Research*, 9, (04), 48662-48672.

INTRODUCTION

Renewable and nonconventional methods of power generation such as wind, solar, hydraulic, biomass, geothermal, thermal storage and waste heat recovery power generations offer power supply solutions for remote areas that are not accessible by grid power supply (Peterseim *et al*., 2014; Zhang *et al*., 2013; Peterseim *et al*., 2014; Srinivas and Reddy, 2014; Iftekhar Hussain *et al*., 2015). Hybrid renewable energy system is an integrated system of two or more renewable energy systems, and can complement each other, provide higher quality and reliable power supply independent of the grid (Peterseim *et al*., 2014; Zhang *et al*., 2013; Peterseim *et al*., 2014; Srinivas and Reddy, 2014; Iftekhar Hussain *et al*., 2015; Department of Energy, 2007; Binayak *et al*., 2014; Kavitha Sirasani and Kamdi, 2013). Hybrid solar/biomass plants will become an increasingly attractive option as the price of fossil fuel and land continue to rise and the cost of solar thermal technology falls (Iftekhar Hussain *et al*., 2015). Although biomass power plants can operate continuously, they can have high initial cost, uncertain supply chain security and require bulk transportation (Srinivas and Reddy, 2014). Mustafa (2013) presented and discussed the electrification of rural area and a review of power standalone system such as; solar and hybrid, solar-wind, solar-hydro hybrid, solar-wind-diesel hybrid, and solar-wind-diesel-hydro/biogas. In addition, reference (Mustafa, 2013) presented and analyzed the viability and importance of solar energy use in global electrification. Another study was proposed by references (Akikur *et al*., 2013) for implementation of hybrid systems in rural area disconnected from the grid. The study discussed two tri-hybridization processes. The tri-hybrid system included hydro-wind and Photovoltaic. A typical hybrid Combined Heat and Power (CHP) system can recover the thermal energy in the fuel flue gas exhaust and converts it into additional electrical energy through a heat engine. Several heat engines have been considered for this type of system including gas turbines, steam turbines and reciprocating engines. A highly efficient and low emitting concept that has been considered for the future is the hybrid gas turbine high temperature (Penyarat Chinda and Pascal Brault, 2012; Dustin McLarty *et al*., 2014; Atideh Abbasi and Zhenhua Jiang, 2008; Yoshimasa Ando *et al*., 2015; Craig S. Turchi and Zhiwen, 2011). The use of binary and Kalina as well as Organic Rankine Cycle (ORC) plants depends on the temperature and state of flue gas flow (Sami, 2011; Sami and Marin, 2016). Of a particular interest is the electrification of remote areas. A review of power stand-alone system that are suitable for electrification of remote areas such as solar and hybrid, solar-wind, solar-hydro hybrid, solar-wind-diesel hybrid, and solar-wind-diesel-hydro/biogas hybrid systems have been presented and discussed in references (Fargali *et al*., 2008; Deissler, 1964). The viability and importance of solar energy use in global electrification also have been presented in that review and analyzed. Another study was proposed by Bhandari (20) for implementation in rural areas disconnected

Corresponding author:* **Sami, S.
Research Center for Renewable Energy, Catholic University of Cuenca, Cuenca, Ecuador

from the grid. The study discussed two tri-hybridization processes. The tri-hybrid system included hydro-wind and Photovoltaic. Furthermore, another PV and hydro-wind system has been suggested to supply uninterrupted power to a remote village in Ethiopia by Bekele and Tedesse (2012). The code HOMER was used to optimize that hybrid system. In addition, other studies were presented on PV-wind-battery hybrid and PV-wind-diesel-battery hybrid intended for rural electrification in Malaysia (Saha *et al*., 2013; Mustafa, 2013; Deissler, 1964; Bekele and Tadesse, 2012; Fadaeenejed *et al*., 2013; Saha *et al*., 2013; Mustafa, 2013; Gherbi, 2013; Sami and Icaza, 2015). Furthermore, the energy conversion equations describing the total power generated by a hybrid system of solar photovoltaic, wind turbine and hydraulic turbine were presented by Sami and Icaza (2015), and integrated simultaneously. For the purpose of validating this simulation model, the energy conversion equations were coded with MATLAB-V13.2. Other hybrid systems were mainly focused on wind energy and its simulation reported in references (Belakehal *et al*., 2010; Murugan *et al*., 2015; Yueqing Zonhan, 2015; Bosma and Kallio, 2009; Ikhsan *et al*., 2013). District heating has cost advantages, and administrative benefits of using a single boiler to provide heat to a number of buildings, individual houses, blocks of social housing, offices (www.districtenergy.org). This paper is concerned with the main heat and mass transfer mechanisms taking place in a hybrid system of biomass based gas turbine and wind turbine for power generation and district heating. A numerical simulation using one dimensional model is presented hereby to describe the process as well as thermal behaviour of associated CHP system.

Mathematical Modeling

In the following sections, the energy conversion equations of the biomass biogas in gas turbine and wind energy into an electrical energy are presented;

Biomass Simulation

In the following the heat and mass transfer model is presented using a gas turbine model where biogas is combusted in the combustion chamber of the gas turbine as illustrated in Figure.1. The flue gas is released from the combustion chamber to the gas turbine where power is produced. The hot flue gas drives an oil loop that drives an Organic Rankine Cycle, ORC. The oil loop is comprised of a tank heat exchanger; ORC waste heat boiler, piping and pump as well as control valves. The radiation is the major heat transfer by-product because of the high temperature of the gas. However, other heat transfer mechanisms are present in the combustion chamber such as convective, evaporation and combustion and must be taken in consideration in order to solve the energy conversion equations of biomass process (Sami and Marin, 2016; Fargali, 2008);

$$Q_{adrin_{gas}} - Q_{adrout_{gas}} = Q_{comb} + Q_{rad} - Q_{conv} - Q_{evap} \quad (1)$$

Where equation (1) can be written in the following form;

$$dT/dt_{oil} = \frac{m_{gas} C_{pgas} (T_{in_{oil}} - T_{out_{oil}})}{V_{tank} \delta_{oil} C_{p_{oil}}} - \frac{m_{oil} C_{p_{oil}} (T_d - T_L)}{V_{tank} \delta_{oil} C_{p_{oil}}} \quad (2)$$

$$Q_{add} = 4.18 C V_{bio} m_{bio} \eta_{heater} \quad (3)$$

$$Q_{conv} = h_w A_{wall} (T_{gas} - T_{well}) \quad (4)$$

$$Q_{rad} = E_g A (T4_a - T4_{bed}) \quad (5)$$

$$Q_{evap} = \eta_{water} H_{evap} \quad (6)$$

dT/dt_{oil}: Represents the time variation of the thermal oil temperature is the heat exchanger tank (see Figure 1).

$$WGT = \eta \, m_{flue\ gas} (h_1 - h_2) \quad (8)$$

Where,

η: is the gas turbine efficiency that takes account various losses during the combustion process.

h_1, h_2: enthalpies of flue gas at inlet and outlet of gas turbine, respectively.

The hot flue gas emitted from the gas turbine is coupled with a thermal oil loop and Organic Rankine Cycle (ORC) to generate refrigerant vapor at waste heat boiler as shown in Figure.1. Interested readers in further details on the use of Organic Rankine Cycle, (ORC), refrigerant mixture fluids as well as their performances, thermodynamic and environmental properties for use in low-temperature organic Rankine cycle systems are advised to consult Sami (Sami, 2011; Sami and Marin, 2016).

The following thermodynamic equations can be written to evaluate the performance of the ORC;

$$W_{ORC} = m_{ref} (h_{orc1} - h_{orc2}) \quad (8)$$

$$Q_{WHB} = m_{ref} (h_{orc1} - h_{orc4}) \quad (9)$$

$$\eta_{ORC} = \frac{W_{ORC}}{Q_{WHB}} \quad (10)$$

$h_{orc\,1}, h_{orc2}$, h_{orc1}, h_{orc4}: enthalpies of refrigerant mixture at inlet, out of vapor turbine, inlet and outlet to waste heat boiler of ORC, respectively.

The refrigerant mixture enthalpies are calculated as per references (Sami, 2011; Sami and Marin, 2016).

Wind turbine Simulation

Wind turbine converts wind energy into mechanical and to electrical energy. The main goal of this model is to optimize the energy conversion from wind energy to electrical energy. Normally, the wind turbine is equipped with a generator with variable speed that synchronize with the wind speed. The output power of the wind turbine is given by the following equation (Kavitha Sirasani and Kamdi, 2013; Mustafa, 2013; Gherbi, 2013; Sami and Icaza, 2015);

$$P_m = \frac{C_p(\lambda,\beta) \rho A}{2 V_W^3} \quad (11)$$

Where, P_m is the mechanical power output of the wind turbine, $C_p, \rho, A \; and \; (\lambda, \beta)$ are the Betz power coefficient, ρ is air density, A is the turbine swept area (m^2) and V_w is the wind velocity. The values $\lambda, and \; \beta$ are the tip speed ratio of rotor blade tip speed to wind speed and blade pitch angle, respectively. λ represents the tip speed ratio of rotor blade tip

speed to wind speed and can be calculated by the following equation (Belakehal *et al*., 2010);

$$\lambda = \frac{R\Omega}{V_W} \quad (12)$$

Where; R represents the radius of the wind turbine blade. Ω is the angular velocity of the rotation of the blades in (rad/s). And $C_P(\lambda, \beta)$ charateristics are defined as follows (Gherbi, 2013);

$$C_P(\lambda, \beta) = c_1 \left(\frac{c_2}{\lambda_i} - c_3\beta - c_4\right) e^{\frac{-c_6}{\lambda_i}} + c_6\lambda \quad (13)$$

Where;

$$\frac{1}{\lambda_1} = \frac{1}{\lambda} + 0.08\beta - \frac{0.035}{\beta^3 - 1} \quad (14)$$

$C_P(\lambda, \beta)$ charateristics were discussed in reference (Gherbi, 2013) for various values β *and*;

The coefficient c_1 through c_6 are as follows (Gherbi, 2013);

$$c_1 = 0.5176, c_2 = 116, c_3 = 0.4, c_4 = 5, c_5 = 21, c_6 = 0.0068 \quad (15)$$

The power output of the wind turbine in equation (11) can be expressed in three-phase power AC as;

$$P_{3f} = \sqrt{3}.\eta_{c1}.U_{line}.I_{line}.Cos\varphi \quad (16)$$

With three phase AC power is P_{3f}, line current I_{line}, represents power factor $Cos\varphi$, and the electric conversion efficiency is referred to as η_{c1}.

Battery charging and discharging Model

The battery stores excess power going through the load charge controller (CF Figure.1-b). The battery keeps voltage within the specified voltage and thus, protects over discharge rates, and prevent overload. During the charging period, the voltage-current relationship can be described as follows (Fargali *et al*., 2008; Mustafa, 2013; Bekele and Tadesse, 2012);

$$V = V_r + \frac{I\left(\frac{0.189}{(1.142 - soc) + R_i}\right)}{AH} + (soc - 0.9)\ln\left(300\frac{I}{AH} + 1.0\right) \quad (17)$$

and;

$$V_r(V) = 2.094[1.0 - 0.001(T - 25°C)] \quad (18)$$

However, during the discharging process and using equation (17), the current-voltage can be;

$$V = V_r + \frac{I}{AH}\left(\frac{0.189}{soc} + R_i\right) \quad (19)$$

And R_i is given by;

$$R_i(\Omega) = 0.15[1.0 - 0.02(T - 25°C)] \quad (20)$$

Where,

$V_r(V)$, I: the terminal voltage and current respectively

$R_i(\Omega)$: Internal resistance of the cell and T is the ambient temperature.

AH: Ampere-hour rating of the battery during discharging process

Charge Controller

Generally, the controller power output is given by (Fargali *et al*., 2008);

$$P_{Cont-dc} = V_{bat}(I_{rect} + I_{wt} + I_{orc}) \quad (21)$$

Where; V_{bat} is multiplication of the nominal voltage DC in the battery for any particular system and I_{rect}, I_{wt} *and* I_{orc} represent the output current of the rectifier in DC and currents of wind turbine and ORC vapor turbine.

Inverter

The characteristics of the inverter are given by the ratio of the input power to the inverter P_{inv-ip} and inverter output powerP_{inv-op}. The inverter will incur conversion losses and to account for the inverter efficiency losses, η_{inv} is used;

$$P_{inv-ip}.\eta_{inv} = P_{inv-op} \quad (25)$$

The AC power of the inverter output P(t) is calculated using the inverter efficiency η_{inv}, output voltage between phases, neutral V_{fn}, for single-phase current I_o and $cos\varphi$ as follows;

$$P(t) = \sqrt{3}\,\eta_{inv}V_{fn}I_o\,cos\varphi \quad (26)$$

Finally, the hybrid system energy conversion efficiency for harnessing energy from wind turbine and Biomass/CHP-ORC is given by;

$$\eta_{system} = \frac{P(t) + Qed}{Qin + Qadd} \quad (27)$$

Where; Q_{in} and Q_{add} are the wind energy and gas turbine combustion heat, respectively. Q_{ed} represents the district heating load.

Numerical procedure

The energy conversion and heat transfer mechanisms taking place during the various processes shown in Figure.1a, and 1-b are described in Equations (1) through (27). These equations have been solved as per the logical flow diagram presented in Figure. 2. The input parameters of Biogas flow rate, wind conditions and the ORC and independent parameters are defined. Dependent parameters were calculated and integrated in the system of finite-difference formulations. Iterations were performed until a solution is reached with acceptable iteration error. The numerical procedure starts with using the wind and biogas flow conditions to calculate the mass flow rates of flue gas, thermal oil, and refrigerant circulating in various loops under specified conditions. The thermodynamic and thermophysical properties of flue gas, thermal oil, and refrigerant are determined based upon the initial conditions of the biogas conditions at the gas turbine compressor inlet, lower

heating value, air flow rate, excess air ratio, and combustion products as well as the ORC output. The flue gas exiting the oil heat exchanger tank is forwarded to the hot water heat exchanger for district heating purposes. Furthermore, it is worthwhile noting that the wind turbine ambient conditions will determine the wind system parameters and output power. Once the ambient conditions were defined this was followed by using the finite-difference formulations to predict the time variation of the oil tank temperature as well as other hybrid system power outputs and efficiencies. Finally, total hybrid system efficiency is calculated at each input condition.

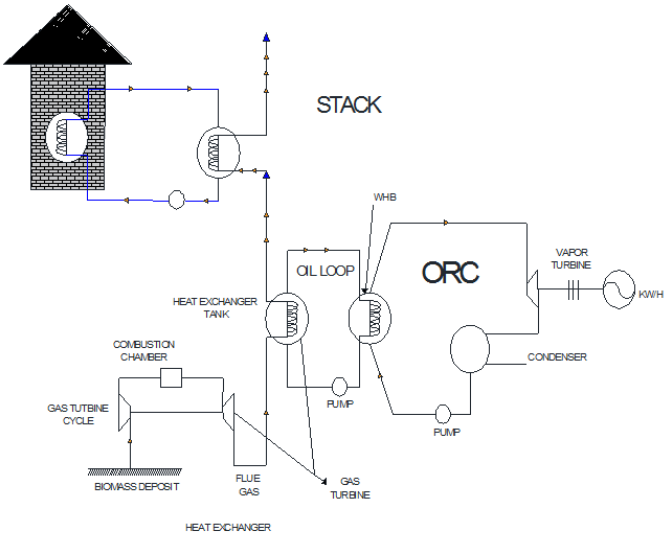

Figure 1-a. Proposed hybrid system Biomass and CHP- ORC subsystem

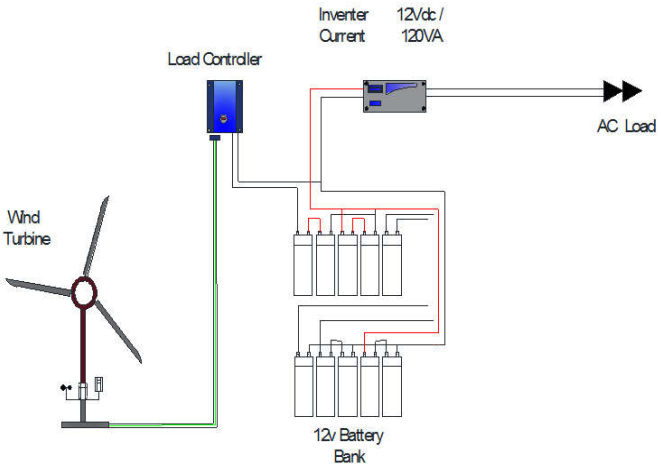

Figure 1-b. Proposed hybrid system wind subsystem

RESULTS AND DISCUSSION

In order to solve the aforementioned equations (1) through (27) and taking into account that total power may not be simultaneous, and for validation purposes, this simulation model and the above mentioned equations were coded with finite-difference formulations. In addition, for the purpose of validation and tuning up the predicted output simulated results, the data was used to validate the simulation program under various conditions. In the following sections, we present analysis and discussions of the numerical results predicted as well as validations of the proposed simulation model.

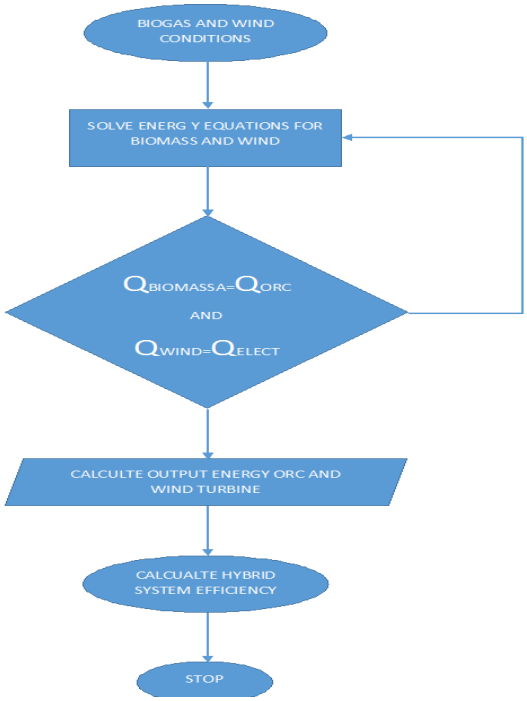

Figure 2. Flow diagram of Hybrid system calculation

Biomass Simulation

Gas turbines have been used to produce power and recently in using biogas in biomass applications. The concept is similar to that of a combustion engine: to convert chemical energy of a fuel biogas into mechanical energy. Air is compressed, fuel is added in the combustion chamber of the gas turbine and the mixture is ignited to initiate combustion. The combustion process releases thermal energy and the air expands and hot flue gases are produced. The flue gases are expended in the turbine and mechanical work is generated out of the cycle. A portion of this mechanical energy is then used to drive the compress the air in the next cycle. As shown in Figure 1-a, the flue gases exiting the gas turbine drive a thermal oil loop which in turn drives the ORC and generate refrigerant superheated vapour. Work is produced at the ORC cycle by expanding the organic refrigerant superheated vapour working fluid in the ORC vapour turbine. On the other hand, the flue gases leaving the thermal oil loop heat exchanger are used to heat up water needed for the district heating process as shown in Figure 1-a.

Equations (1) through (10) present the heat and mass calculation balance at the combustion chamber of the gas turbine where the biogas is fed the gas turbine combustion chamber and during this process the combustion heat is released and heats up the flue gases. It is well known that increasing the excess air results in decreasing the combustion gas temperature (Sami, 2011; Sami and Marin, 2016). The predicted results of the biomass simulation at different conditions are presented in Figures 3 through 7. In particular, figures 3 and 4 depict the biomass total output power at the ORC generator end and the gas turbine using the biogas at different flow rates as well as different flue gas temperatures. It is quite evident from the simulation data presented in these figures that biogas with higher flues gas temperatures increases the output power and similarly higher flue gas flow rates increase the biomass process total output power. Similar behavior was observed at other biogas flow rates and flue gas

temperatures. In addition, the results in the aforementioned figures also show that the higher biomass heat supplied the higher output power generated at the ORC. Since higher and lower temperatures of at the ORC do not change, only increasing the heat input at the gas turbine combustion chamber increases the heat losses and consequently the biomass energy conversion efficiency as outlined in equation (1). As previously discussed, the higher the furnace gas exit temperature results in higher biomass efficiency since because of complete combustion and the destruction of incomplete combustion products (ICP) and full burning. And the data also presented in these figures illustrate that the higher the biomass loading the higher the efficiency.

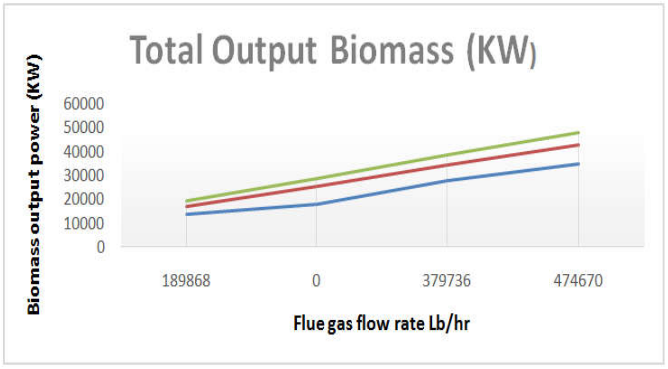

Figure 3. Biomass output power at different biomass flows

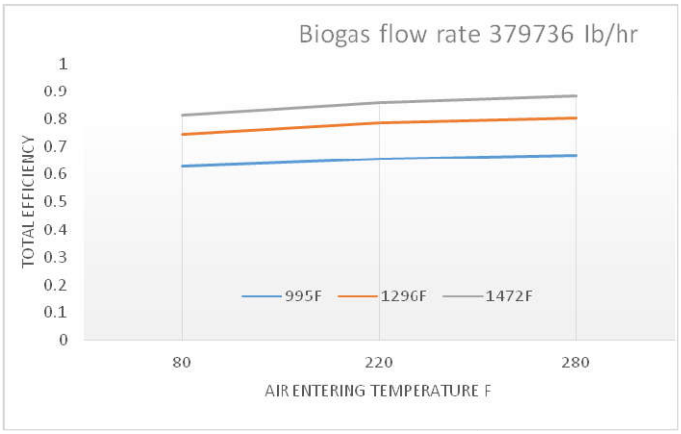

Figure 4. Biomass output Efficiency at different air entering temperature

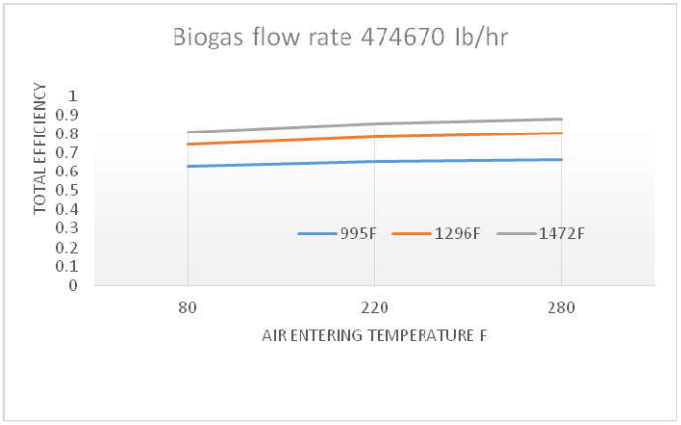

Figure 5. Biomass efficiency at different biomass different air entering temperature

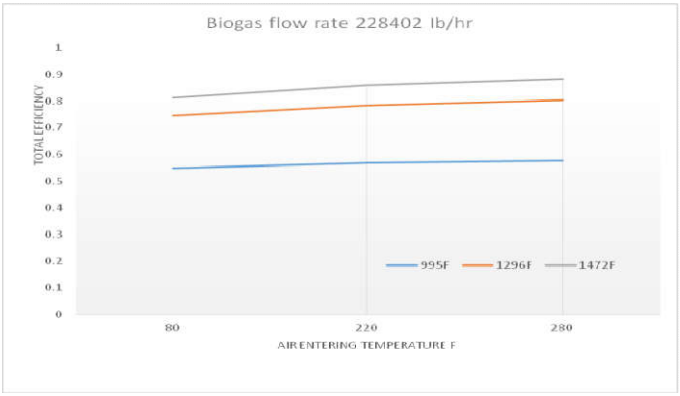

Figure 6. Biomass efficiency at different biomass different air entering temperature

Furthermore, in order to study the impact of the time-variation of initial oil temperature on the energy conversion process, Figure .7 has been constructed. The dynamic behavior of the thermal oil medium used to transfer the heat from the biomass flue gas to the ORC can be predicted by equation (2) and is shown in Figure. 7 for various biomass flow rates. It is quite clear from this figure that the maximum allowable temperature should not be exceeded (550 F). This is important since beyond this temperature the Dow thermal oil considered in this simulation could disintegrate and compromise the heat transfer process in the Waste heat boiler as shown in Figure 1. It is also evident from the data displayed in this Figure that at a particular time the lower the biogas flow rate the higher the oil temperature supplied to the ORC waste heat boiler and obviously the higher the ORC output power produced. It is also clear from this figure that according the design criteria of the ORC conditions, the supply oil temperature should not be lower than 450 °F which is achieved after 4 hours and below this temperature the ORC system output will not be viable. This is significant since normally the lower oil supply temperature to ORC is critical condition to generate vapor refrigerant at the waste heat boiler and consequently power at the vapor turbine to avoid supplying the ORC vapor turbine with vapor under saturated vapor conditions.

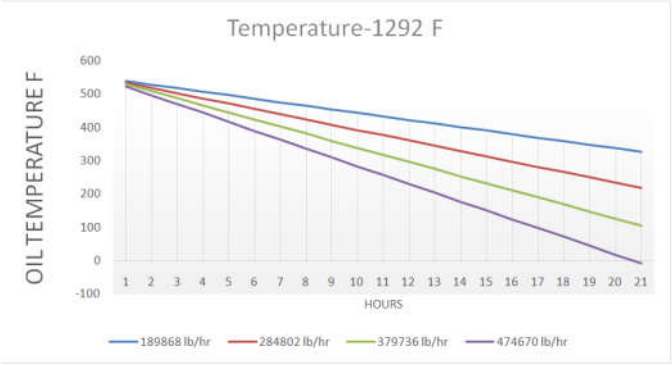

Figure 7. Time-variation of heat transfer fluid temperature at different biogas flow rates

District Heating Simulation

District heating is significantly used European countries where there are a number of successful district heating applications using biomass and CHP plants (Ikhsan *et al*., 2013). A typical district heating installation uses hot water or steam to heat up the buildings and using a heat exchanger within each building

(C.F. figure 1-a). In this paper, the flue gas exhausting the biogas gas turbine is employed to heat up the heating water circulating in the buildings. Significant number of installations operates district heating plants by Energy Service Companies (ESCOS). As presented in this paper elsewhere, district heating is provided using the co-generated heat from electrical power generation in a Combined Heat and Power (CHP) installation. This is very beneficial since it can enhance the overall efficiency of power generation of the hybrid system and will be demonstrated elsewhere in this paper. To this end, Figure. 8 has been presented to show the effect of changing the biogas mass flow rate on the building heating load at different flue gas flow rates exhausted from the turbine as shown in Figure.1-a. It is evident from the results presented in this figure that the higher the biogas mass flow rate the higher the heat supplied to the building. It is quite important to highlight that the building heating load is dependent upon the outdoor conditions and consequently varies as these conditions vary will impact the ORC output power.

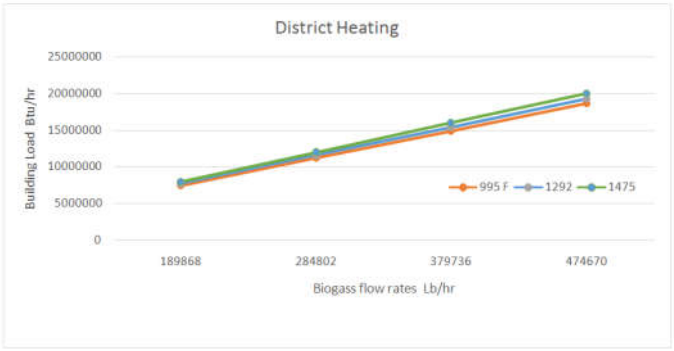

Figure 8. District heating building load Btu/hr.

Wind Turbine Simulation

As discussed and presented in equations (11) through (16) the wind turbine power is significantly influenced by the Betz Coefficient $C_P(\lambda,\beta)$ and the function (λ,β) represents the tip speed ratio of rotor blade and blade pitch angle. The wind turbine under consideration is compromised of nose cone, three blades, hub, generator, rotor diameter of 3.2 meter, three reinforced fiber glass blades. The rated power is 1500 watts and maximum power reported by manufacturer is 1800 watts (Yueqing Zonhan, 2015). Therefore, it with current geometries the wind turbine rated power can be achieved with β=0 and λ=12. On the other hand, Figure. 9 has been constructed to illustrate the dependence of the Betz coefficient on those parameters at different values of β and λ. It is quite clear from the data displayed in this figure that the maximum value of the Betz coefficient is obtained at β and λ values of 0 and 8.1, respectively. In Figures 10 through 12, we have examined the wind power predicted at various β and λ ranging from 0 to 15 and 5 to 12, respectively for wind turbine for the wind turbine aforementioned characteristics. Furthermore, with current rotor geometry the maximum wind can be achieved at speed of 11 m/s and β=0 and λ=12 as shown in Figure.10. However, it appears that the maximum wind power can be achieved theoretically by altering the rotor geometry as presented in Figure 12 with β= 15, λ=8.1.

Furthermore, Figures. 13 through 15 have been presented to show the impact of Betz Coefficient $C_P(\lambda,\beta)$ characteristics on the wind turbine efficiency at different wind speed. It is evident from data displayed in these figures that the higher the blade pitch angle the higher wind turbine efficiency. However, the results displayed in this figure showed that at higher wind velocity of 11 m/s wind power and wind turbine efficiency is maximized at can be attained at λ and β of 8.1 and 15 respectively. On the other hand, Figures 16 through 18 demonstrate the importance of wind speed on the hybrid system efficiency as defined by equation (27). The simulation results presented in these figures illustrate that at λ=5 the wind speed impact on the hybrid system efficiency is insignificant. However, the greater impact was observed at λ=8.1 in Figure. 17. Therefore, in order to maximize the hybrid system efficiency, the tip speed ratio of rotor blade should be λ=8.1.

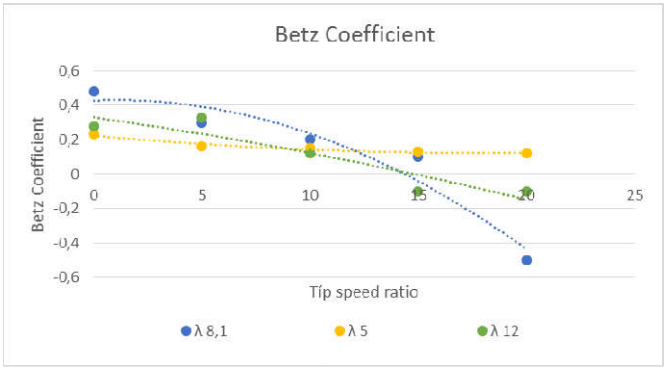

Figure 9. Betz Coefficient $C_P(\lambda,\beta)$ characteristics at various wind speed and blade pitch angle

Furthermore, in order to study the impact of varying the biogas flow rates on the hybrid system total efficiency, Figures 19 through 21 were plotted at λ=8.1 and various wind speed values. The results depicted in the these figures clearly illustrate that at a specific speed and β and λ values , the higher the biogas flow rate the lower the lower the hybrid system total efficiency. Therefore, the aforementioned suggests that at specific wind speed the hybrid system total efficiency can be optimized by selecting the appropriate biogas flow rate. This provides an important guidance to the designers for the optimization of hybrid systems composed of biogas gas turbine, wind turbine and district heating.

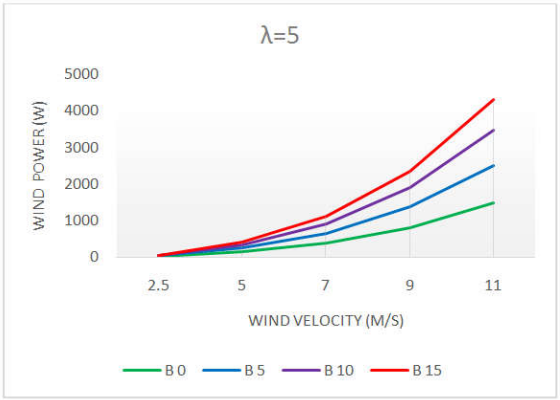

Figure 10. Wind Power for different values of wind speed and $C_P(\lambda,\beta)$

As previously discussed the power of the hybrid system under investigation is also significantly influenced by the Betz Coefficient $C_P(\lambda,\beta)$ as well as the biogas flow rates. Furthermore, the hybrid total efficiency is also impacted by other parameters such as flue gas temperatures.

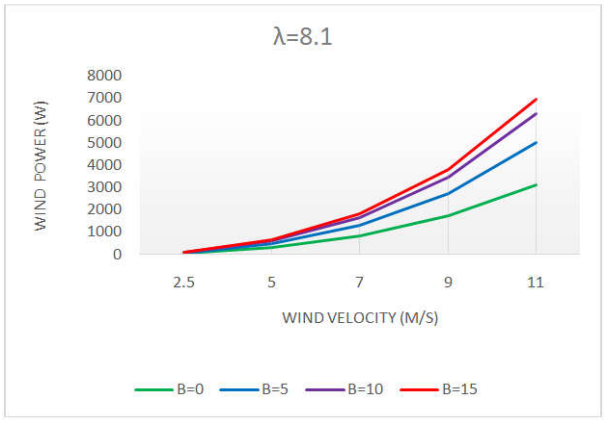

Figure 11. Wind Power for different values of wind speed and $C_P(\lambda, \beta)$

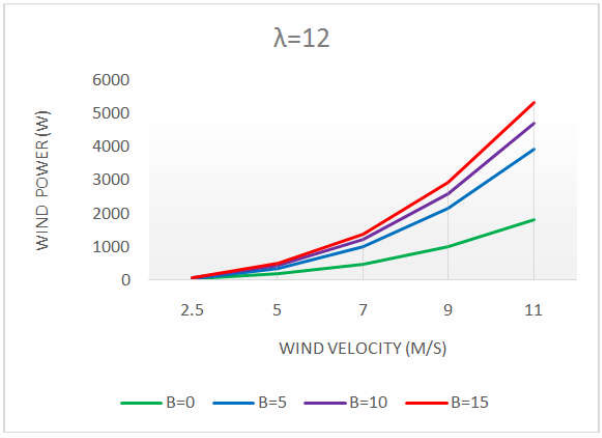

Figure 12. Wind Power for different values of wind speed $C_P(\lambda, \beta)$

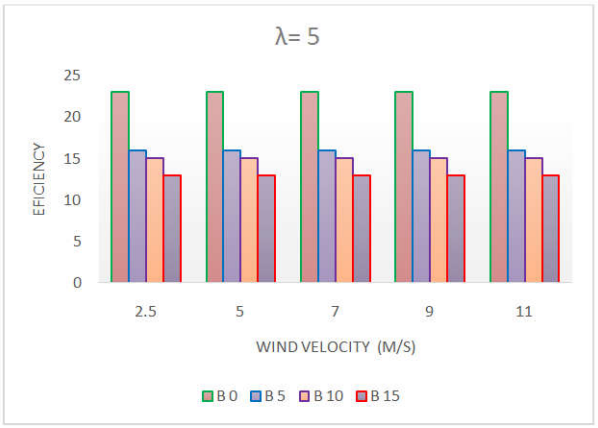

Figure 13. Wind turbine efficiency for different values for λ=5

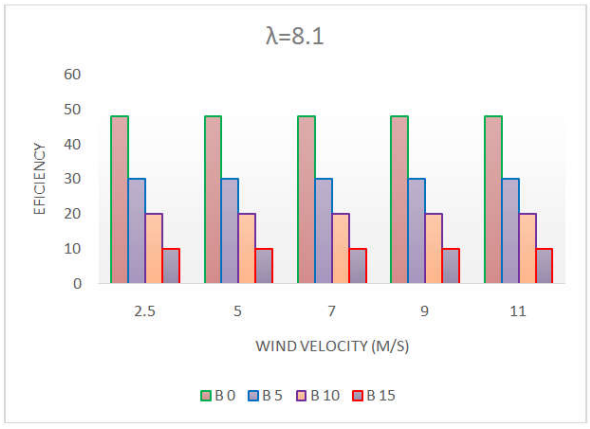

Figure 14. Wind turbine efficiency for λ=8.1

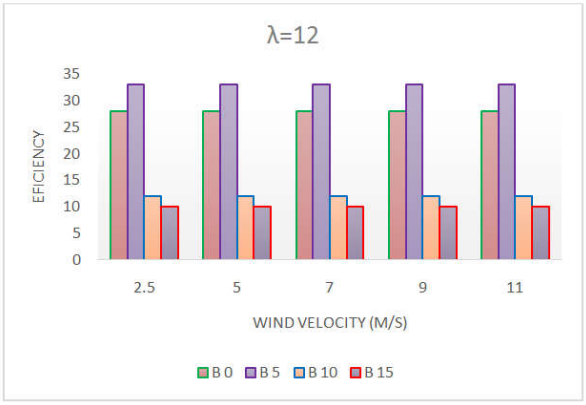

Figure 15. Efficiency of wind turbine at λ=12

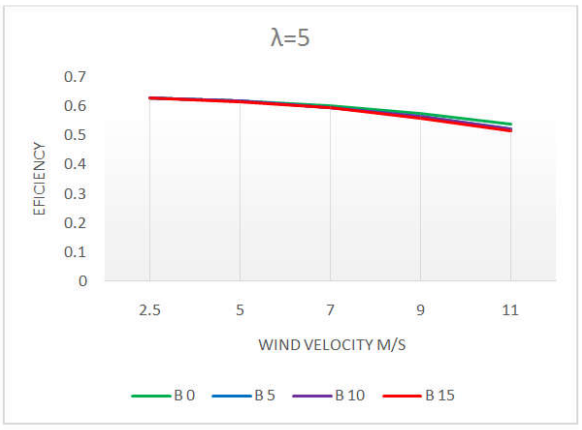

Figure 16. Hybrid system efficiency of wind turbine at λ=5

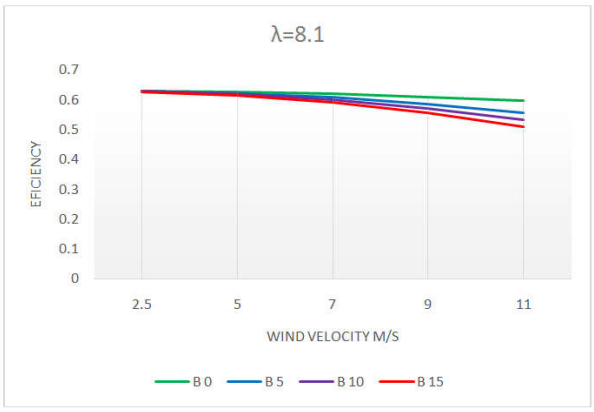

Figure 17. Hybrid system Efficiency of wind turbine at λ=8.1

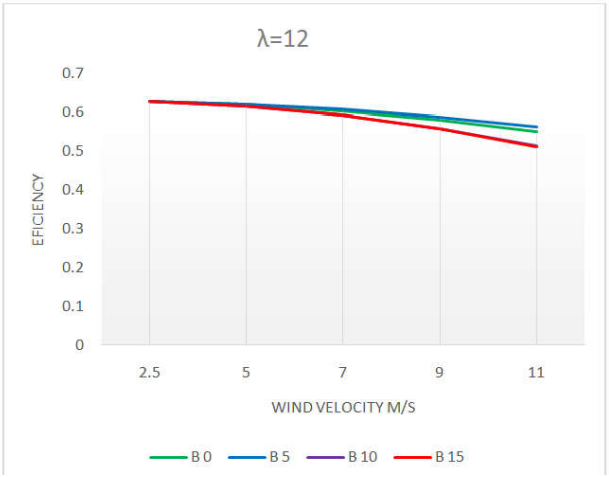

Figure 18. Hybrid system efficiency of wind turbine at λ=12

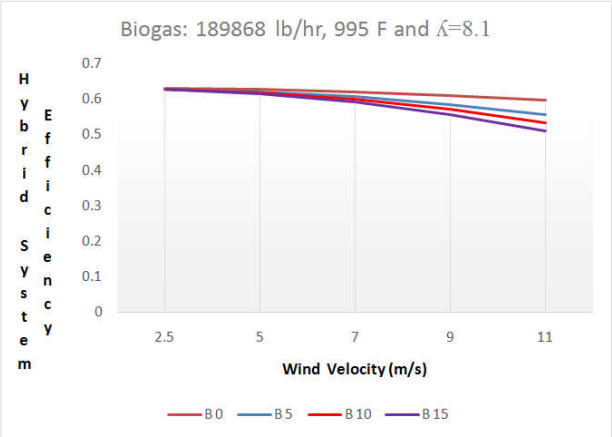

Figure 19. Hybrid system efficiency at λ=8.1 and flue gas temperature 995 F

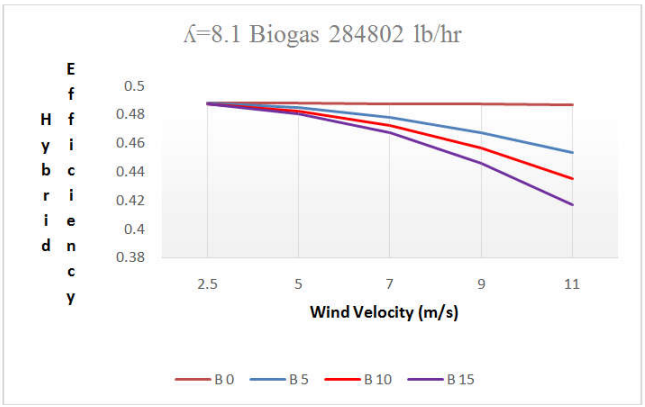

Figure 20. Hybrid system efficiency at λ=8.1 and flue gas temperature 995 F

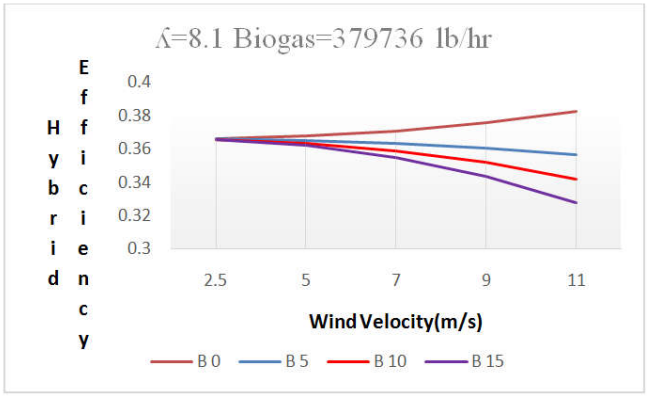

Figure 21. Hybrid system efficiency at λ=8.1 and flue gas temperature 995 F

Therefore, Figures 22 and 23 were constructed to illustrate the impact of these parameters on the hybrid system efficiency. These figures were constructed under optimum performance with function(λ, β), 8.1 and 0, respectively and different biogas flows and wind velocities. It can be observed from these figures that at a lower biogas flow rate, the higher the wind velocity the lower the hybrid system efficiency. This is attributed to the fact that wind turbine efficiency is significantly lower than the efficiencies of the gas turbine/CHP and the ORC. However, it can be seen that higher biogas flows result in insignificant changes in the hybrid system efficiency under higher wind speeds. This is also can be attributed to the fact that higher biogas flows increases heat of combustion in the combustion chamber and the flue gas temperature. Furthermore, it was also observed that the higher the flue gas temperature exiting the combustion chamber, the lower the hybrid system efficiency under higher wind speeds.

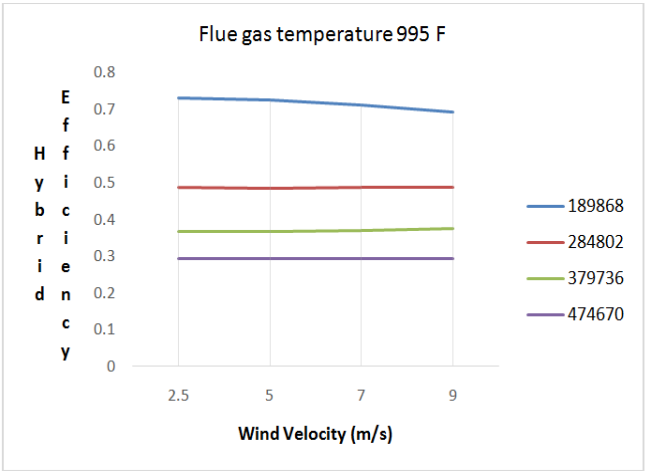

Figure 22. Hybrid system efficiency at λ=8.1 and β flue gas temperature 995 F for different mass flow rates (lb/hr

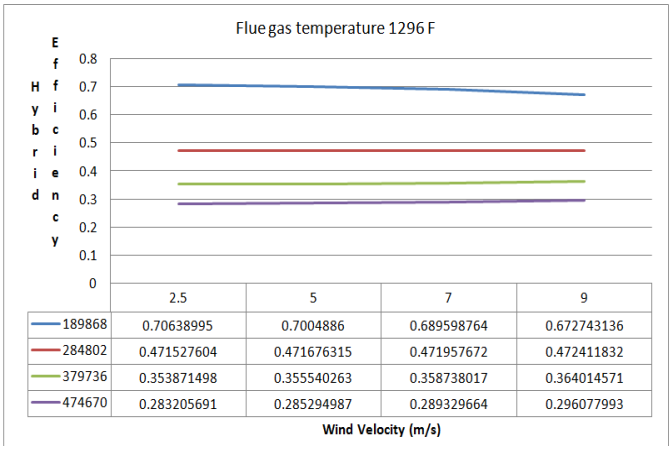

	2.5	5	7	9
189868	0.70638995	0.7004886	0.689598764	0.672743136
284802	0.471527604	0.471676315	0.471957672	0.472411832
379736	0.353871498	0.355540263	0.358738017	0.364014571
474670	0.283205691	0.285294987	0.289329664	0.296077993

Figure 23. Hybrid system efficiency at λ=8.1 and β flue gas temperature 1296 F for different mass flow rates (lb/hr)

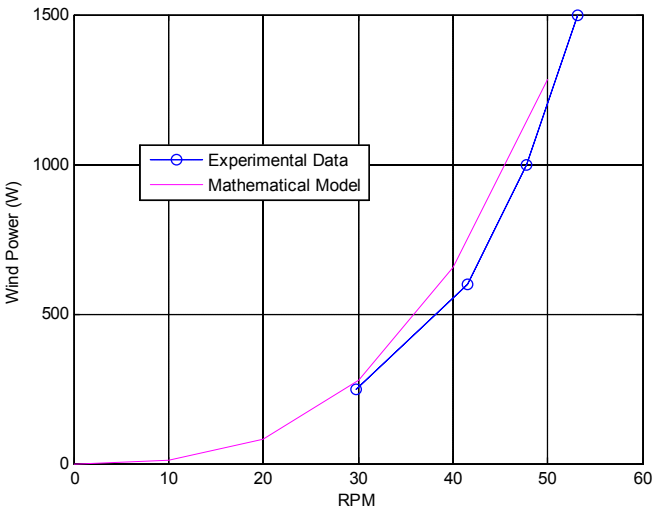

Figure 24. Comparison between Wind Turbine data Bosma and Kallio (2009) and model prediction (Sami and Icaza, 2015)

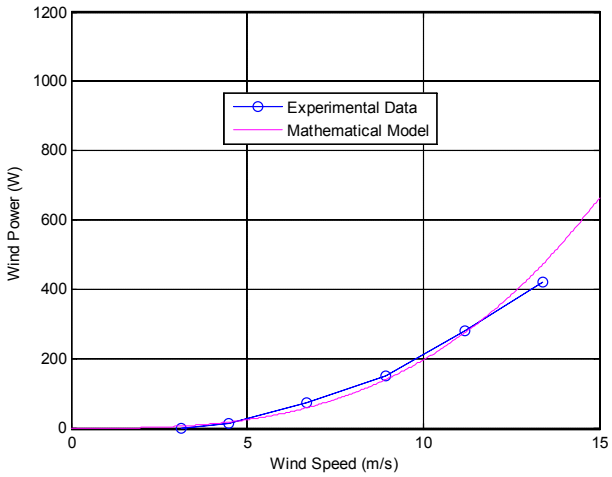

Figure 25. Comparison between Wind Turbine data (Ikhsan *et al*. (2013)) and model's prediction (Sami and Icaza, 2015)

Validation of Simulation Model

In order to validate our numerical model prediction described in equations (1 through 27), we have constructed Figures 24 and 25 to compare the predicted results by our simulation model with data presented in the literature on wind turbine only since literature data were very limited to wind turbine data and none was available for biomass gas turbine using biogas for comparison purposes. Thus, the experimental data presented by references (Bosma and Kallio, 2009) and (Ikhsan *et al*., 2013) for wind turbines were used for validation purposes. Figures 24 and 25 show a comparison of the predicted output powers of the wind turbine under investigation (Bosma and Kallio, 2009; Ikhsan *et al*., 2013) against the experimental data at various wind speed and RPM of the turbine shaft. In Figure 24 the wind turbine data presented by Bosma and Kallio (2009) were displayed, simulated and compared to our numerical model's prediction at different RPM. It is quite apparent from this figure that our numerical model fairly predicted the wind turbine output power. However, further analysis of figure. 25 points out that our model predicted very well the wind power data up to wind speed of 5.5 m/s. However, beyond that point there was some discrepancies between the model prediction and the data. We believe these discrepancies are due to variable Betz coefficient $C_P(\lambda, \beta)$ and kinetic and mechanical losses at higher wind speeds. In addition, since our model assume a constant Betz coefficient, our model could not take into account the mechanical and kinetic losses encountered at high speed.

Conclusions

The energy conversion equations describing the total power generated by a hybrid system of wind turbine aero generator, biomass integrated biogas turbine-ORC and district heating have been coded, solved and presented. The biomass data also illustrates that the higher the biomass biogas flow the higher the efficiency.

Furthermore, the wind turbine study results showed that the higher the wind velocity the higher the output power, however, the output power is critically dependent upon the Betz coefficient which is a function of the wind turbine geometrical configuration. It is imperative that the design of the wind turbine takes into consideration the geometry of the wind turbine blades and the site wind conditions as well as the ambient temperatures. Finally, the model prediction compared fairly with the wind turbine data at different conditions. Finally, this study revealed that at a lower biogas flow rate, the higher the wind velocity the lower the hybrid system efficiency.

Nomenclature

A is the turbine swept area (m^2
$C_{p_{oil}}$: Specific heat of thermal oil
C_p: Specific heat of Flue gas
CV_{bio}: Calorific heat value of bio-gas
h_w: Convection heat transfer coefficient
h_1: Enthalpy of refrigerant at vapor turbine entrance
h_2: Enthalpy at exit of vapor turbine
h_4: Enthalpy at inlet of waste heat boiler
H: Convective heat transfer coefficient
Q_{comb}: Combustion heat added
Q_{rad}: Radiative heat
Q_{conv}: Convective heat
Q_{evap}: Evaporative heat
T: is the temperature thermal oil in heat exchanger tank
Vw: Wind speed
V: The output voltage of the PV array and approximately equal to the battery voltage.
V_{tank}: Volume of heater
m_{gas}: Mass flow rate of flue gas
m_{bio}: Biomass waste mass material
m_{ref}: Mass flow rate ORC cycle refrigerant
W_{ORC}: Work generated at ORC vapor turbine generator
Q_{WHB}: Heat transferred from thermal oil to refrigerant at the waste boiler heat exchanger

Greek alphabet

λ= Tip speed ratio of rotor blade tip speed to wind speed
β= Blade pitch angle,
ρ_{air}= Air density.
η_{inv}= Inverter efficiency
η_{ORC}: ORC thermal efficiency
η_{bio}: Biomass furnace efficiency

Subscripts:

$bat -$ Battery
$inv - ip$ - Inverter input
$inv - op$ - Inverter output
p – Power
$total$ – Total
$3f$ – Three phase AC

Acknowledgement

The research work presented in this paper was made possible through the support of the Catholic University of Cuenca.

REFERENCES

Akikur, R.K., Saidur, R., Ping, H., Ullah, K.R. 2013. "Comparative Study of Stand-Alone and Hybrid Solar Energy Systems Suitable for Off-Grid Rural electrification:

A review", Renewable and Sustainable Energy Reviews, Vol. 27, 738-752.

Atideh Abbasi and Zhenhua Jiang, 2008. Design and analysis of a fuel cell/gas turbine hybrid power system, Power and Energy Society General Meeting - Conversion and Delivery of Electrical Energy in the 21st Century, 2008 IEEE

Bekele, G and Tadesse, G. 2012. "Feasibility Study of Small Hydro/PV/Wind Hybrid System for off- Grid Rural Electrification in Ethiopia", Applied Energy, Vol 97, pp.5-15.

Belakehal, S., Bentounsi, M., Merzoug, and Benalla, H, 2010. "Modeling and Control of a Permanent Magnetic Synchronous Generator Dedicated to the Conversion of Wind Energy", *Journal of Renewable Energies*, Vol. 13, No. 1, 149-161,

Bhandari, B. 2014. "Design and Evaluation of tri-hybrid Renewable System (THRES)," Ph. D. Thesis, Department of Mechanical & Aerospace Engineering, Seoul National University.

Binayak, B., Shiva, R. P., Kyung-Tae L., Sung-Hoon A. 2014. "Mathematical Modeling of Hybrid Renewable Energy System: A Review on Small Hydro-Solar-Wind Power Generation", *International Journal of Precision engineering and Manufacturing-green Technology*, Vol. 1, No 2, pp. 157-173.

Bosma B. and Kallio G. 2009. "Renewable-energy labs for an undergraduate energy-systems course", American Society for Engineering Education.

Bosma B. and Kallio G. 2009. "Renewable-energy labs for an undergraduate energy-systems course", American Society for Engineering Education.

Craig S. Turchi, and Zhiwen M, Gas Turbine/Solar Parabolic Trough Hybrid Designs, to be presented at the ASME Turbo Expo 2011, Vancouver, Canada, June 6-10, 2011

Deissler, G. 1964. "Diffusion approximation for thermal radiation in gases with jump boundary conditions" *ASME Journal of Heat Transfer*, Vol 86, 240-246, 1964.

Department of Energy, "Potential Benefits of Distributed Generation and Rate Related Issues that may Impede their Expansion, A Study Pursuant to Section 1817 of the Energy Policy Act of 2005" 2007.

Dustin McLarty, Jack Brouwer, Scott Samuelsen, 2014. Fuel cell–gas turbine hybrid system design part I: Steady state performance, *Journal of Power Sources*, Volume 257, 1 July, Pages 412–420

Fadaeenejed, M, Radzi, M. A., AbKadir, M.Z. and Hizam, H. 2013. "Assessment of Hybrid Renewable Power Sources for Rural Electrification in Malaysia", Renewable and Sustainable Energy Reviews, Vol. 30, pp. 299- 305.

Fargali, H., M., Fahmy, F.H. and Hassan, M.A. 2008. "A Simulation Model for Predicting the Performance of PV/Wind- Powered Geothermal Space Heating System in Egypt", The Online Journal on Electronics and Electrical Engineering (OJEEE), Vol.2, No.4.

Gherbi, A. 2013. "Modeling and Simulation of Hybrid Systems (PV/Wind/Battery) connected to the Grid', ICEEAC 2013, International Conference on Electrical Engineering and Automatic Control, Setif, 24-26 November.

Howell, J. R., R. B. Bannerot, and G. C. Vliet, 1982. Solar-Thermal Energy Systems: Analysis and Design, McGraw-Hill, Inc., New York.

Iftekhar Hussain, C.M. Duffy, A. and Norton, B. 2015. "A Comparative Technological Review of Hybrid CSP-Biomass CHP Systems in Europe", International Conference on Sustainable Energy & Environmental Protection, Paisley, UK, 11-14 August

Ikhsan*, M., Agus Purwadi, Nanang Hariyanto, Nana Heryana, Yanuarsyah Haroen" 2013. Study of Renewable Energy Sources Capacity and Loading Using Data Logger for Sizing of Solar-Wind Hybrid Power System" 4th International Conference on Electrical Engineering and Informatics (ICEEI 2013)

Ikhsan*, M., Agus Purwadi, Nanang Hariyanto, Nana Heryana, Yanuarsyah Haroen, 2013. "Study of Renewable Energy Sources Capacity and Loading Using Data Logger for Sizing of Solar-Wind Hybrid Power System" 4th International Conference on Electrical Engineering and Informatics (ICEEI 2013)

Kavitha Sirasani and S.Y. Kamdi, 2013. "Solar Hydro Hybrid Energy System Simulation" *International Journal of Soft Computing and Engineering (IJSCE)*, Volume-2, Issue-6, pp. 500-503, January,

Murugan, N, Umamaheswari, M., Vimal, SI. and Sivashanmugam, P. 2015. "Experimental Investigation on Power Output in Aged Wind Turbines", *Advances in Mechanical Engineering*, Volume 2012, Article ID 380986, 7pages, July.

Mustafa E. 2013. "Sizing and Simulation of PV-Wind Hybrid Power System", *International Journal of Photoenergy*, Volume, ID 217526, pp.1-10, 2013.

Mustafa, E. 2013. "Sizing and Simulation of PV-Wind Hybrid Power System", *International Journal of Photoenergy*, Vol 2013, Article ID 217526, 10 pages.

Mustafa, E. 2013. "Sizing and Simulation of PV-Wind Hybrid Power System", *International Journal of Photoenergy*, Vol 2013, Article ID 217526, 10 pages.

Penyarat Chinda and Pascal Brault, 2012. The hybrid solid oxide fuel cell (SOFC) and gas turbine (GT) systems steady state modeling, *International Journal of Hydrogen Energy*, Volume 37, Issue 11, June, Pages 9237–9248

Peterseim JH, White S, Tadros A, Hellwig U. 2014. "Concentrating solar power hybrid plants -Enabling cost effective synergies. Renew Energy; vol. 67: pp178 –85.

Peterseim. J. H, Hellwig. U, Tadros. A, White. 2014. "Hybridisation optimization of concentrating solar thermal and biomass power generation facilities", *Science direct Solar Energy,* vol. 99, pp. 203– 214.

Saha, N.C., Acharjee, S., Mollah, M.A.S., Rahman, K.T. and Rafi, F. H. M. 2013. "Modeling and Performance Analysis of a Hybrid Power System", Proc. of International Conference on Informatics Electronics & Vision (ICIEV), pp. 1-5.

Saha, N.C., Acharjee, S., Mollah, M.A.S., Rahman, K.T., and Rafi, F. H. M. 2013. "Modeling and Performance Analysis of a Hybrid Power System", Proc. of International Conference on Informatics Electronics & Vision (ICIEV), pp. 1-5.

Sami, S. 2011. "Behaviour of ORC low Temperature Power Generation with Different Refrigerants" *International Ambient Energy Journal*, Volume 32, No.1.

Sami, S. and Icaza, D. 2015. "Modeling, Simulation of Hybrid Solar Photovoltaic, Wind turbine and Hydraulic Power System", IJEST, *International Journal of Engineering Science and Technology*, Volume 7, Issue 9, September 30.

Sami, S. and Marin, E. 2016. "A Numerical model for predicting performance of biomass and CHP hybrid system", under press.

Srinivas. T. and Reddy B.V. 2014. "Hybrid solar -biomass power plant without energy storage", Reference:

CSITE22, Appeared in: Case Studies in Thermal Engineering, 23 January.

www.districtenergy.org

Yoshimasa Ando, Hiroyuki Oozawa, Masahiro Mihara, Hirroki Irie, Yasutaka Urashita, Takuo Ikegami, Demonstration of SOFC-Micro Gas Turbine (MGT), Mitsubishi Heavy Industries Technical Review Vol. 52 No. 4 (December 2015)

Yueqing Zonhan Wind Power Co. Ltd., "Operating & Installation Manual", ZH1.5 kw wind turbine system. 2015.

Zhang HL, Baeyens J, Degreve J, Caceres G. 2013. "Concentrated solar power plants: review and design methodology". Renew Sustain Energy Review, vol.22, 446-481.

****